

Fusing Multisource Data to Estimate the Effects of Urbanization, Sea Level Rise, and Hurricane Impacts on Long-Term Wetland Change Dynamics

David F. Muñoz ^{ID}, Paul Muñoz ^{ID}, Atieh Alipour ^{ID}, Hamed Moftakhar ^{ID}, Hamid Moradkhani ^{ID}, and Behzad Mortazavi ^{ID}

Abstract—Wetlands are endangered ecosystems that provide vital habitats for flora and fauna worldwide. They serve as water and carbon storage units regulating the global climate and water cycle, and act as natural barriers against storm-surge among other benefits. Long-term analyses are crucial to identify wetland cover change and support wetland protection/restoration programs. However, such analyses deal with insufficient validation data that limit land cover classification and pattern recognition tasks. Here, we analyze wetland dynamics associated with urbanization, sea level rise, and hurricane impacts in the Mobile Bay watershed, AL since 1984. For this, we develop a land cover classification model with convolutional neural networks (CNNs) and data fusion (DF) framework. The classification model achieves the highest overall accuracy (0.93), and f1-scores in woody (0.90) and emergent wetland class (0.99) when those datasets are fused in the framework. Long-term trends indicate that the wetland area is decreasing at a rate of $-1106 \text{ m}^2/\text{yr}$ with sharp fluctuations exacerbated by hurricane impacts. We further discuss the effects of DF alternatives on classification accuracy, and show that the CNN & DF framework outperforms machine/deep learning models trained only with single input datasets.

Index Terms—Data fusion, deep learning, hurricane impacts, mobile bay, sea level rise, urban development, wetland loss.

I. INTRODUCTION

WETLANDS are defined as lands transitional between terrestrial and aquatic ecosystems [1] that provide valuable services to society [2]. Among those services, wetlands improve water quality due to their capacity for nutrient and pollutant removal [3], [4]. Wetlands regulate the global climate through carbon sequestration and methane emissions [5]–[7], and also

Manuscript received October 14, 2020; revised December 16, 2020; accepted December 29, 2020. Date of publication January 1, 2021; date of current version January 21, 2021. This work was supported in part by the National Science Foundation INFEWS Program under Award EAR-1856054. (Corresponding author: David F. Muñoz.)

David F. Muñoz, Atieh Alipour, Hamed Moftakhar, and Hamid Moradkhani are with the Department of Civil, Construction and Environmental Engineering, and the Center for Complex Hydroystems Research, The University of Alabama, Tuscaloosa, AL 35487 USA (e-mail: dfmunoz1@crimson.ua.edu; aalipour@crimson.ua.edu; hmoftakhar@eng.ua.edu; hmoradkhani@ua.edu).

Paul Muñoz is with the Departamento de Recursos Hídricos y Ciencias Ambientales, Universidad de Cuenca, Cuenca, EC 35487, Ecuador (e-mail: paul.munozp@ucuenca.edu.ec).

Behzad Mortazavi is with the Department of Biological Sciences, and the Center for Complex Hydroystems Research, The University of Alabama, Tuscaloosa, AL 35487 USA (e-mail: bmortazavi@ua.edu).

Digital Object Identifier 10.1109/JSTARS.2020.3048724

contribute to maintaining biodiversity [8]. In coastal systems, wetlands act as water-storage units regulating the global water cycle and providing flood mitigation services such as storm-surge, wave attenuation, and hurricane protection [9]–[11].

Despite the ecosystem services they provide, wetlands are frequently threatened by anthropogenic activities including water abstraction and pollution, deforestation, intensive agriculture, aquaculture, and urban development [12], [13]. Wetlands are also vulnerable to natural disasters such as erosion, droughts, sea level rise (SLR), and hurricane impacts among other complex stressors, many of which are exacerbated by climate change [14], [15]. Previous estimates indicate that since 1900 nearly 70% of global natural wetlands have disappeared with a rate of almost four times faster in the 20th and early 21st centuries than previously [16]. Estimation of wetland loss attributed to SLR is challenging in absence of high-resolution digital elevation models (DEMs), flood-protection infrastructure delineation, and accurate land cover maps that help understand wetland dynamics in response to rising sea levels [17], [18]. Besides SLR, hurricanes are responsible for coastal wetland erosion that directly depends on impact duration, wind strength, speed of the storm, and the relative distance of wetland regions to the hurricane track [19], [20].

In the Conterminous United States (CONUS), the “Status and Trends of Wetlands: 2004–2009” report indicates that freshwater wetland loss was mainly attributed to silviculture practices (56%) and urban development (23%), whereas coastal (marine and estuarine) wetland loss was associated with wetland conversion into deepwater bay bottoms or open ocean (83%) [14]. Likewise, nearly all of the estuarine emergent wetland loss (99%) was attributed to coastal processes including saltwater inundation and storm-surge. At the regional scale, Ellis *et al.*, [21] conducted a land cover land use change (LCLUC) assessment in the vicinity of Mobile Bay, AL for the period 1974–2008. They indicated that nonwoody wetlands decreased by 6.4% ($\sim 10 \text{ km}^2$) whereas woody wetlands increased by 3.4% ($\sim 26 \text{ km}^2$) with respect to 1974. The authors used Landsat imagery of Mobile and Baldwin counties and produced LCLUC maps based on a three-stage classification approach and machine learning (ML) techniques (e.g., decision tree and unsupervised/supervised classification). A detailed description of this approach was later presented by Spruce *et al.* [22]. Both studies reported moderate to high overall accuracies (OAs) in the land cover classification process (83% to 91%).

Significant improvements in LCLUC assessment have been reported when integrating ML with hierarchical classification strategies and object-based image analysis [23], [24]. However, deep convolutional neural networks (CNNs) outperform traditional (shallow) ML approaches (e.g., random forest, support vector machine, and decision tree) in a variety of applications including object detection, segmentation and spatial structure pattern analyses [25], [26]. CNNs are state-of-the-art machine learning techniques that use a deep architecture characterized by multiple layers, nonlinear functions, and parameter-sharing that allow for optimal feature learning at low-, mid-, and high-levels of abstraction (i.e., edges, object parts, and patterns). Thus, CNNs achieve high performances in image recognition and classification tasks [27], [28]. Furthermore, integrating CNNs and geo-spatial data fusion (DF) of multisource and multisensor data can improve complex land cover classification in urban and natural (wetland) landscapes.

Chen *et al.* [29] proposed deep CNNs and DF of multi-hyperspectral imagery (HSI) and light detection and ranging (LiDAR) data for accurate classification of urban landscapes. The authors developed a feature fusion framework consisting of a bi-branch CNN architecture that extracts spatial-spectral features from HSI and spatial-elevation features from LiDAR data. More advanced CNN & DF frameworks that integrate HSI and LiDAR data with very high-resolution imagery (VHI) were evaluated in the 2018 IEEE GRSS Data Fusion Contest [30]. The contest winner team proposed a fully connected convolutional network (Fusion-FCN) that reduces the risk of spatial information loss and improves the classification accuracy via post-classification processing. The Fusion-FCN approach consists of three branches that extract features from VHI+LiDAR intensity, LiDAR-derived digital surface maps and HSI, separately. Recently, Feng *et al.* [31] proposed a novel alternative for DF of multisource HSI and LiDAR data based on “Squeeze-and-Excitation Networks” [32]. The alternative consists in an adaptive feature-fusion approach that evaluates the importance or contribution of each feature to the final classification task (i.e., feature weights), and thereby fusing multisource features in a more intelligent fashion than the two CNN architectures aforementioned. Regarding natural landscapes, Pouliot *et al.* [33] performed an assessment of CNNs for wetland mapping using Landsat imagery. The authors developed a Multi-Size/Scale ResNet Ensemble approach and evaluated wetland detection accuracy at different sampling spatial extents (e.g., local and regional level), since spectral characteristics might vary over large study areas. The CNN & DF frameworks described above were used for short-term land cover classification (e.g., up to three years) and proved the benefits of DF in complex urban and wetland classification.

Despite those efforts, research to date has not yet determined a suitable framework for long-term studies. This study therefore aims at contributing to this growing area of research by developing a land cover classification (LCC) model with a tri-branch CNN architecture and the adaptive feature-fusion approach for optimal DF. Moreover, in this study, we attempt for the first time a long-term (35-year) analysis that includes the effects of three major drivers, namely urbanization, sea level rise, and hurricane

impacts. We combine multiannual imagery and generic DEMs for wetland cover change analysis in the Mobile Bay watershed, AL. Specifically, we use readily available datasets consisting of the following:

- 1) satellite-based Landsat imagery;
- 2) airborne imagery of the National Agriculture Imagery Program (NAIP); and
- 3) LiDAR-derived DEMs corrected for wetland elevation error [24].

The LCC model is trained with land cover maps of the National Land Cover Database (NLCD) [34] and validated with maps of both the NLCD and the Coastal-Change Analysis Program (C-CAP) [35].

II. STUDY AREA AND MATERIAL

A. Study Area

Mobile Bay is located in southwestern Alabama, U.S. [see Fig. 1(a)]. In terms of freshwater influx, Mobile Bay is the fourth largest estuary in the CONUS with a mean daily freshwater discharge of 1715 m³/s [36]. This relatively shallow estuary has a mean depth of 3 m and connects the Mobile Bay watershed and the Gulf of Mexico through a narrow inlet between Dauphin Island and Fort Morgan Peninsula. Freshwater discharge at the head of the estuary comes from the Tensaw River and Mobile River, which conveys ~95% of the freshwater inflow to the bay [37]. The Mobile Bay watershed has a surface area of ~2261 km² and comprises Bon Secour Bay (southeast) and the Gaillard Island (northwest) created with dredged material in 1979. In addition, Weeks Bay located upstream of Bon Secour Bay is a tributary estuary of Mobile Bay that has been designated as National Estuarine Research Reserve.

B. Data Availability

The LCC model processes two imagery datasets of moderate (30 m) to very high (0.5–1 m) spatial resolution and LiDAR-derived DEMs of high spatial resolution (3 m) (see Table I). The first dataset consists of Landsat Analysis Ready Data (ARD) available at the Earth Explorer website.¹ This dataset contains scenes (path 21, row 38) collected around the growing (leaf-on) and hurricane seasons (June to November). We selected (single) annual Landsat ARD scenes with cloud cover and shadow less than 20% and close to hurricane landfall dates. Although time series analysis with several scenes of the same year may improve the accuracy of the LCC model, such an analysis is not always possible due to cloud formation during the hurricane season.

Landsat ARD scenes are already corrected for atmospheric attenuation including scattering and absorption effects [38], which can substantially lower the accuracy of classification tasks [39]. Consequently, we will not conduct analyses with Landsat scenes in the period 1974–1983 as they are not corrected for atmospheric attenuation. The second dataset consists of airborne NAIP imagery from the United States Department of Agriculture archive² and collected from 2006 to 2019 over Mobile and

¹[Online]. Available: <https://earthexplorer.usgs.gov>

²[Online]. Available: <https://nrcs.app.box.com/v/gateway>

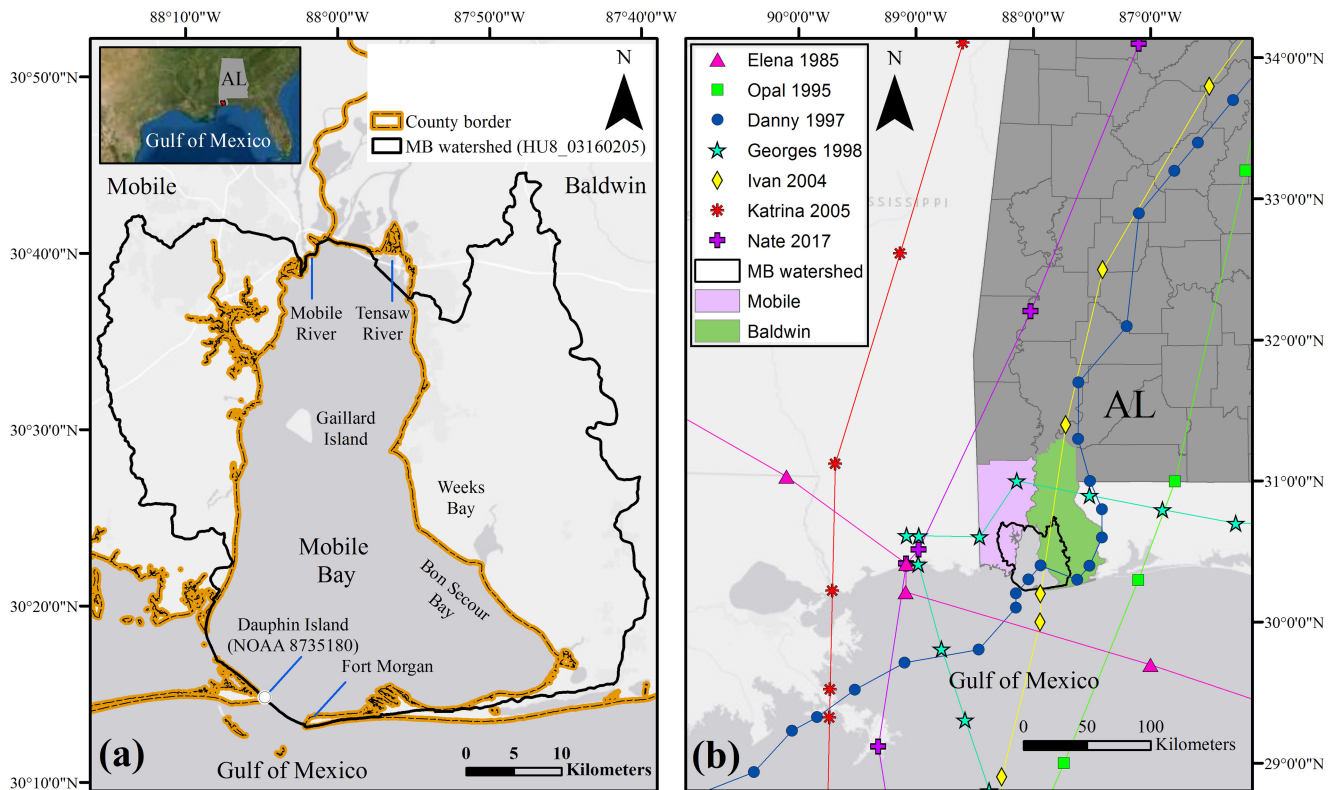


Fig. 1. Map of Mobile Bay, AL. (a) Mobile Bay watershed and county borders between Mobile (west) and Baldwin (east) counties. (b) Hurricane best tracks denote 6-hour intervals and landfall close to Alabama State in the past four decades.

TABLE I
SELECTED DATASETS TO TRAIN AND VALIDATE THE LAND COVER CLASSIFICATION (LCC) MODEL

Dataset	Resolution [m]	Time frame	Bands
Landsat (ARD)	30	1984 to 2019	Red, green and near-infrared
NAIP	0.50 and 1	2006, 2009, 2011, 2013, 2017 and 2019	Red, green and blue
LiDAR-derived DEM	3	1988 - 2013	
C-CAP	30	1996, 2001, 2006, 2010, 2015 and 2016	Single band
NLCD	30	1992, 2001, 2004, 2006, 2008, 2011, 2013 and 2016	

Baldwin counties during leaf-on conditions (or growing season). Both imagery datasets are selected for this study as they complement each other in terms of temporal and spatial resolution. Landsat has a revisit time of 15 days, whereas NAIP provides imagery with a frequency of 2 to 5 years. Moreover, NAIP imagery is not often explored in deep learning (DL) applications despite its potential for very high spatial resolution mapping and land cover classification [40].

The third dataset consists of generic DEMs created with the most updated LiDAR-derived DEM of the Northern Gulf of Mexico (NGOM), which can be obtained from the NOAA's Data Access Viewer website.³ The NGOM DEM consists of multisource topographic and bathymetric elevation data (topo-bathy) including LiDAR point clouds, hydrographic, multibeam

and side-scan sonar surveys collected from 1888 to 2013. The generic DEMs are referenced with respect to the North American Vertical Datum 1988 (NAVD88) and corrected for wetland elevation error as further described in Section III-A. In addition to those datasets, the LCC model is trained with land cover maps of the NLCD⁴ and validated with maps of both the NLCD and C-CAP archives.⁵ The NLCD is a multitemporal database of the conterminous United States that consists in a comprehensive data analysis of Landsat imagery and ancillary datasets with image segmentation, decision tree classification techniques, and a postclassification refinement process [34]. The C-CAP monitors changes of coastal intertidal areas, wetlands, and adjacent uplands based on automated classification of high-resolution NAIP

³[Online]. Available: <https://coast.noaa.gov/dataviewer/#>

⁴[Online]. Available: <https://www.mrlc.gov/data>

⁵[Online]. Available: <https://coast.noaa.gov/digitalcoast/tools/lca.html>

imagery, available LiDAR digital elevation data, and assorted ancillary information. C-CAP produces LCLUC products for coastal regions of the United States every five years.

III. METHODOLOGY

A. Wetland Elevation Correction and Generic DEMs

Several studies have reported that LiDAR-derived DEMs contain surface elevation errors (i.e., vertical bias) in coastal wetlands [41]–[43], especially in salt marsh species where overestimation of true elevation can be as high as 0.65 m [44]. Similarly, Muñoz and Moftakhari [24] reported an overestimation of salt marsh elevation (e.g., emergent herbaceous wetlands) up to 0.50 m in Weeks Bay of the NGOM DEM. The authors estimated vertical bias with a “DEM-correction” tool that automates the elevation correction process based on the spatial distribution of emergent herbaceous wetlands from C-CAP, NLCD, and updated wetland maps. Specifically, the tool modifies an existing DEM through linear elevation adjustment and site-specific parameters [17] and was validated with publicly available real-time kinematic elevation data. Furthermore, the DEM-correction tool was used in other studies for an accurate representation of wetland elevation, which in turn improved the accuracy of compound flooding and velocity maps from hydrodynamic simulations [10]. The DEM-correction tool is used to create generic DEMs for Mobile Bay watershed based on the existing NGOM DEM along with eight available NLCD and C-CAP maps (see Table I). Since C-CAP maps offer a detailed land cover classification with multiple categories [35], we reclassify and match these categories to the land cover classes established in the NLCD [1], [34]. Specifically, we group “palustrine” and “estuarine” wetland categories (C-CAP) into “woody” or “emergent herbaceous” wetlands (NLCD) based on the classification criteria of both maps [45]. Subsequently, we use the DEM-correction tool to address vertical bias in emergent herbaceous wetlands and produce eight generic DEMs with corrected elevation features within these wetlands. Although the remaining land cover classes might have considerably changed through time; and thereby requiring similar alternatives for elevation correction, we show that spatial–spectral features of multiannual Landsat/NAIP imagery help overcome misclassification errors associated with misleading elevation features of the generic DEMs (see Section III-B2 for details). Since we are particularly interested in changes of wetland distribution, the resulting generic DEMs can be seen as a proxy of historical wetland elevation maps that are often scarce. Table II summarizes the generic DEMs and presents DF alternatives based on available datasets.

B. Land Cover Classification (LCC) Model

1) *Data Preprocessing:* We conducted a correlation analysis between the multispectral bands from Landsat ARD imagery to select optical bands with the least redundant information for model training and finetuning of the CNN architecture. The band selection technique was used in similar studies for complex land cover and wetland classification with satisfactory

TABLE II
GENERIC DEMS CREATED WITH THE DEM-CORRECTION TOOL ALONG WITH C-CAP AND NLCD MAPS. DATASET COMBINATIONS WITH/OUT GENERIC DEMS INDICATE DATA FUSION ALTERNATIVES

Land cover map	Time frame	Dataset combination
n/a (without DEM)	1984, 1986, 1988, 1989, 1993, 1994, 1995, 1997, 1998, 1999, 2002, 2005, 2007, 2014 and 2018	ARD
	2009, 2017 and 2019	ARD + NAIP
	1996, 2010 and 2015	ARD + DEM
C-CAP	1992, 2001, 2004, 2008 and 2016	ARD + DEM
NLCD	2006, 2011 and 2013	ARD + NAIP + DEM

results in model learning optimization, computation burden and/or graphics-processing-unit memory usage reduction [26], [46]. Particularly, we used the “band collection statistics” tool in ArcGIS and found the highest average band correlation between the blue and red bands (0.91). Therefore, we considered the nir, red, and green bands of Landsat ARD imagery and the red, green, and blue bands of NAIP imagery in the CNN & DF framework (see Fig. 2).

Since the coarser resolution of C-CAP and NLCD maps is 30 m, the LCC model may be trained with “patch” images of 30×30 m for pixel-based validation. However, DL models that are trained with a pixel-based approach cannot learn contextual information from local spatial features of neighboring pixels [27], [29]. Moreover, data segmentation and the whole learning process could be computationally expensive. Therefore, we first resampled all datasets to a pixel resolution of 5 m with the “nearest neighbor” method and then rescaled data values to a range of 0 and 1. Although a higher pixel resolution (e.g., 1 m) would contain detailed spatial–spectral information of NAIP imagery, there is always a tradeoff between accuracy and computation burden in land cover classification at large scale. Likewise, we opted for a patch-based (instead of a pixel-based) approach centered on a single pixel to train and validate the model. This approach relies on the first law of geography where neighboring pixels are likely to belong to the land cover class of the central pixel [47]. As a result, the LCC model assigns a unique class label for all pixels inside a given patch image.

Furthermore, the size of patch images (i.e., “ $h \times w$ ” shown in Fig. 2) plays a key role in classification accuracy and depends on the resolution and size of the input datasets [29], [48], as well as the size of target objects (e.g., salt marsh platforms, mangrove ponds, crop parcels, etc.). In general, oversized patches add more noise than local information, lead to undersegmentation problems and reduce OAs regardless of the CNN architecture [27], [31], [33]. We conducted trial-and-error tests with randomly generated patch sizes ranging from 10 and 50 pixels, and found that the optimal patch size and shape that prevents overfitting and undersegmentation is a square patch of 30×30 pixels. Similarly, other studies reported an identical patch size and shape for complex land cover and wetland mapping [26], [46].

2) *Convolutional Neural Network and Multisource Data Fusion:* The LCC model uses a CNN & DF framework resembling the Fusion-FCN architecture presented in the 2018 IEEE GRSS Data Fusion Contest [30] and the adaptive feature-fusion

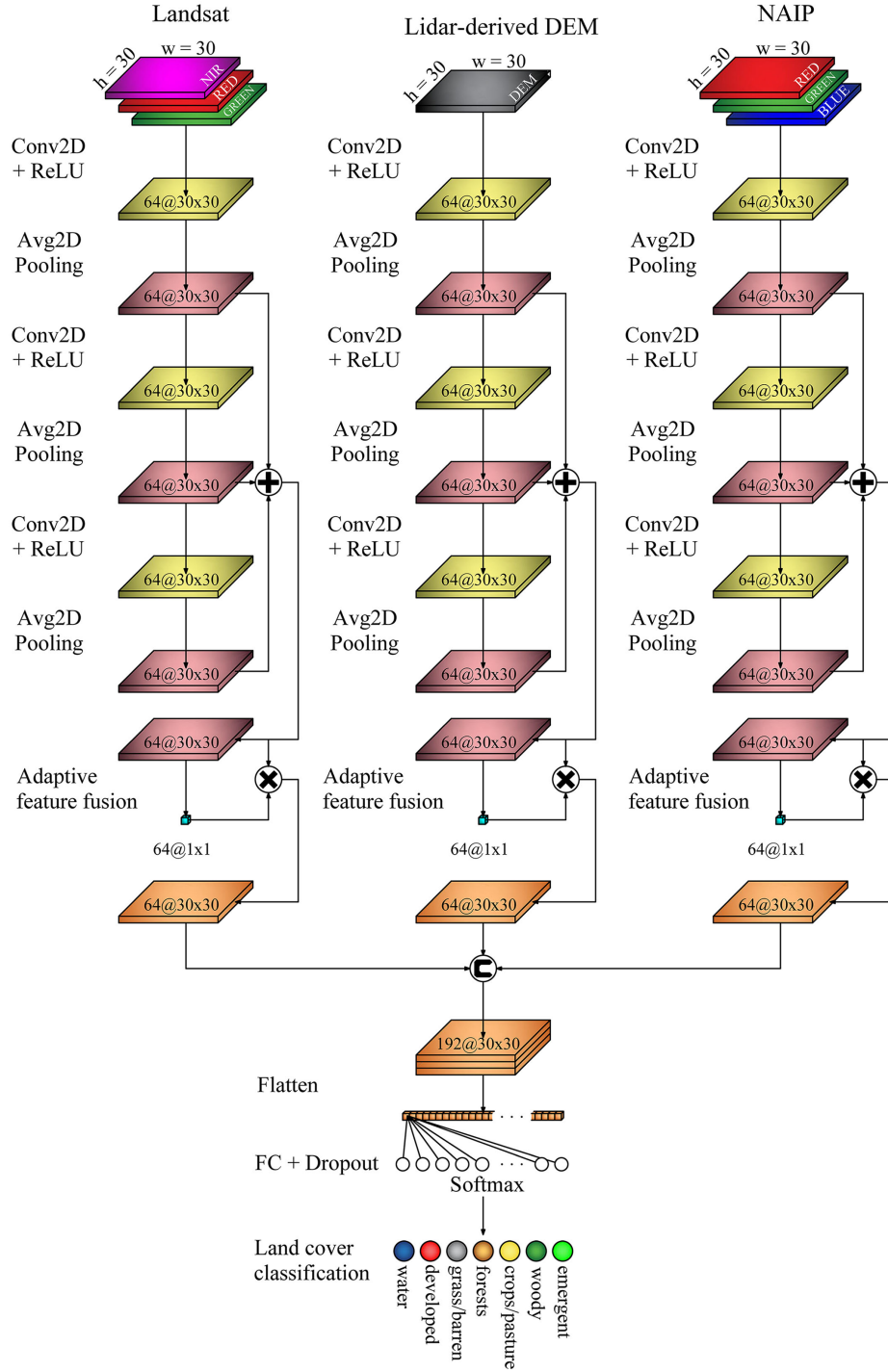


Fig. 2. Land cover classification (LCC) model based on convolutional neural networks (CNN) and multi-source data fusion (DF). The model consists of a tri-branch CNN with 2D convolution (Conv), rectified linear unit (ReLU) and average (Avg) pooling operations. Avg2D pooling layers are merged into a single layer through point-wise addition (+), whereas the adaptive feature-fusion module is implemented for optimal DF. Feature weights are assigned to the Avg2D pooling layers through the point-wise product (X), and subsequently concatenated (C) and flatten. Land cover classification is ultimately conducted with a fully connected layer, dropout and ‘Softmax’ function.

approach [31]. The framework is developed in TensorFlow (www.tensorflow.org) and consists of a tri-branch CNN architecture that processes Landsat, LiDAR-derived DEM and NAIP datasets simultaneously (see Fig. 2). The left and right branches process patch images of three spectral bands from Landsat (nir, red, and green) and NAIP (red, green, and blue) datasets,

respectively, while the middle branch extracts spatial-elevation features from LiDAR-derived DEM data of single bands. Along each branch, three sets of 2-D convolution (Conv), rectified linear unit (ReLU), and average (Avg) pooling operators extract feature information from patch images of 30×30 pixels at low-, mid-, and high- levels of abstraction. We set two kernel sizes of

3×3 and 2×2 for Conv2D and Avg2D pooling operations, respectively, and use “same” (zero) padding at the boundaries to preserve the input shape ($h \times w$) of patch images. In addition, we add batch normalization layers at the beginning of each branch and after each Conv2D layer to accelerate the learning process [49], lower the “dropout” rate and control overfitting [27]. Moreover, model weights of all set of layers (e.g., kernel and bias) are randomly initialized using a “glorot uniform” scheme and zero-values, respectively, to achieve a higher model convergence [50]. We then merge the resulting Avg2D pooling layers into a single layer through point-wise addition, and hence benefit from multiscale properties along each branch. Since CNN architectures are flexible in terms of the amount of layers and kernel sizes, we previously evaluated the layer sets in the CNN & DF framework (see Section IV-A for details).

Next to that, we integrate the adaptive feature-fusion approach [31] in the CNN architecture. The approach requires a 2-D global average pooling layer (Gap2D), two fully connected (FC) layers and a “Sigmoid” function. A detailed description of those layers are presented in the Appendix (see Table VI). The resulting output tensor contains the global contribution of each input layer to the land cover classification task (i.e., feature weights). These weights are subsequently assigned to the input layers of each branch through the point-wise product (or scalar multiplication), and the three weighted layers are concatenated and flatten for optimal DF as shown in Fig. 2. As the final step, we add a FC layer with dropout rate set to 0.2 and a “Softmax” function for final land cover classification. The dropout method inactivates a given percentage of neurons to prevent complex co-adaptations in CNNs and helps prevent overfitting [29], [51]. We transform the 15 land cover classes originally established in the Mobile Bay watershed [52] into 7 generalized categories to avoid unnecessary specificity given the ultimate goal of our study. In that regard, similar wetland cover change studies used a more general classification scheme to improve LCLUC interpretability [21], [22], [33].

3) *Model Training and Validation:* The CNN & DF framework is trained and validated in two steps: 1) pretraining the tri-branch CNN architecture before the adaptive feature-fusion approach and 2) finetuning the entire CNN architecture with single, double, and triple datasets depending on data availability. The first step consists in training each branch independently by leveraging all available validation maps per dataset and then saving model weights of each set of layers (e.g., kernel and bias) for further use in the CNN & DF network. For instance, the left branch (Landsat imagery) counts with eight NLCD and three C-CAP maps that can effectively be used to train and validate the LCC model (see Table II). Similarly, the middle branch can leverage those 11 maps for DEM generation accordingly (see Section III-A). Note that the left branch can process nine NAIP imagery datasets (see Table I), but there are only three existing land cover maps readily available for training and validation purposes.

Before training the model, we compute the class weights of each land cover class to deal with unbalanced data and use a sample size of 25% of the input datasets. We then randomly separate training (80%) and validation (20%) datasets and

ensure reproducibility with a fixed seed value. The LCC model uses the stochastic gradient descent algorithm with exponential decay and the sparse categorical cross-entropy loss as the model optimizer and loss function, respectively. The model is trained with 100 epochs and “early stopping” set to 10 epochs to avoid overfitting. In addition, we set an initial learning rate of 0.01 and 0.001 for imagery and DEM datasets, respectively. The learning rate and number of training epochs are selected from trial-and-error tests with randomly selected values ranging from 0.0001 to 0.1 and 50 to 200, respectively, whereas the remaining parameter-values are based on similar CNN model settings reported in recent literature [26], [27], [29], [46].

In the second step, we integrate the pretrained branches with the adaptive feature-fusion approach according to the DF alternatives presented in Table II. In that sense, the model can adaptively identify land cover classes in absence of Landsat ARD, NAIP or DEM data, or alternatively, incorporate other datasets (if available) under additional branches. We conduct finetuning of the entire CNN architecture with an initial learning rate of 0.001 and identical model setting and parameter-values as previously described. The model weights obtained from finetuning are then saved along with those of the set of layers. Specifically, we use the model weights in the CNN & DF framework to generate land cover maps with input datasets that lack NLCD and C-CAP maps or validation data. In other words, the framework leverages pretrained model weights of multiannual data to accurately identify land cover classes with unused Landsat ARD, NAIP, or generic DEM datasets.

The LCC model is validated with selected patch images of 30×30 pixels (see Section III-B1 for details) obtained from NLCD and C-CAP maps around the Mobile Bay watershed. Particularly, we ensure that patch images representing woody and emergent herbaceous wetlands match the NAIP imagery of very high spatial resolution. Moreover, we allow the patch images to contain less than 90 pixels (or $<10\%$) of other land cover classes (e.g., open water, forest, developed areas, etc.) in an attempt to control misclassification errors arising from patches centered at the edge of two or more classes. The latter also augment the number of patches per land cover class and indirectly helps mitigate unbalanced class problems. The resulting land cover maps have a spatial resolution of 30×30 m by setting an overlap of 6 pixels in x - and y -direction (i.e., strides) for all patches of ARD, NAIP, and DEM datasets. We ultimately implement post-classification processing to ensure correct mapping of small streams and river branches often misclassified as wetlands. Also, we ensure that transport infrastructure (e.g., highways and second-order roads) are correctly delineated in the land cover maps.

4) *Wetland Cover Change Analysis:* For this analysis, we define urbanization, SLR and hurricane impacts to any gain or loss of developed, open water and remaining land cover class areas, respectively, with respect to existing wetland cover areas. We analyze their effects on wetland cover change using a total wetland distribution expression:

$$Tw = U + S + C \quad (1)$$

where Tw is the total wetland balance (i.e., gain or loss) in km^2 , U , S , and C are wetland net gains or losses attributed to urbanization

TABLE III
ACCURACY ASSESSMENT OF DATA FUSION ALTERNATIVES FOR MULTI-ANNUAL (2006, 2011, AND 2013) LAND COVER CLASSIFICATION

Dataset	Overall Accuracy (%)	Cohen's kappa (%)	f1-score (macro) (%)
Landsat (ARD)	85.36	82.51	83.25
NAIP	74.56	69.55	72.12
LiDAR-derived DEM	73.90	68.31	56.70
ARD + NAIP	87.88	85.53	85.76
ARD + DEM	89.83	87.82	85.69
NAIP + DEM	89.48	87.42	86.49
ARD + NAIP + DEM	93.24	91.93	92.01

(developed class), SLR (open water class) and the remaining land cover classes, respectively.

The overall effect of hurricane impact on coastal wetlands is implicit in the variables S and C as strong winds, high storm-surge, or torrential rainfalls cause severe wetland and shoreline erosion, denude marshes, create ponds, and deposit sediments in the interior of marshes [19]. A detailed analysis of hurricane effects on wetland coverage within those two variables is beyond the scope of this study. We use land cover maps generated with the CNN & DF framework and geo-spatial analysis to compute (1). The effect of urbanization on wetland cover change (loss/gain) can be estimated by identifying wetland areas altered to/from developed areas in the given 5-year interval. The difference between wetland gain and loss is the net residual attributed to urbanization (U). Since the developed class consists of various categories (e.g., open space, low, medium, and high intensity areas), we may obtain a wetland gain in developed areas; especially in open space areas that are suitable for upland wetland migration [53], [54]. For a detailed description of land cover classes, the reader is referred to the 2016 NLCD classification system and legend [52]. Similarly, the effects of SLR on wetland coverage can be estimated with an identical analysis with the open water class of NLCD and C-CAP maps. For simplicity, we assume that net residuals obtained from open water class (S) involve complex processes such as salinization, sediment deposition, and nutrient availability that directly affect wetland biomass productivity, and thus wetland dynamics [55]–[57]. The last variable (C) can be computed following the geo-spatial analysis described above for the remaining land cover classes.

IV. RESULTS

A. Model Performance and Accuracy Assessment

We evaluate model performance and compare the benefits of DF alternatives in terms of OA, f1-score (macro-average and per-class) Cohen's kappa coefficient and confusion matrix. We did not find any significant improvement of OAs and f1-scores when including additional Conv2D and Avg2D pooling layers in the CNN & DF framework, but rather observed an increase of computational burden and time. Likewise, we evaluated both kernel sizes as well as the number of kernel filters after each Conv2D+ReLU operation. There was no improvement of OAs and f1-scores with kernel filters beyond 64 and kernel sizes larger than 3×3 . We select three years that contain all input datasets and validation maps readily available (e.g., 2006, 2011, and 2013) and compute evaluation metrics with a sample

size of 25% per dataset as described in Section III-B3. The highest accuracies are achieved when the three datasets are fused together as indicated in Table III.

Fusing either Landsat ARD or NAIP imagery with generic DEM data leads to similar accuracies with a slightly better model performance of ARD + DEM. Although ARD has a coarser spatial resolution than NAIP (i.e., five times factor), spatial-elevation features from the generic DEMs help overcome the spatial resolution difference between these imagery datasets. This is also noticeable when comparing the former DF alternatives against ARD + NAIP, which shows a reduction of $\sim 2\%$ of OA and Cohen's kappa. The generic DEMs provide a correct representation of historic emergent herbaceous wetland distribution and elevation using the NGOM DEM regardless of the other land cover classes. Nevertheless, fusing both spatial-elevation with spatial-spectral features helps improve OAs of ARD and NAIP imagery in $\sim 5\%$ and $\sim 15\%$, respectively. When comparing the evaluation metrics of each dataset in isolation, ARD outperforms NAIP despite the coarser spatial resolution. This in turn reveals that the band selection technique (see Section III-B1) among optical bands of Landsat ARD improves model performance in more than 10% when compared to NAIP datasets. Besides, ARD dataset in isolation achieves similar accuracies compared to previously proposed geospatial LCLUC methods for Mobile Bay [22]. DEM data in isolation reaches similar accuracies than NAIP, but f1-score (macro-average) metric shows a reduction of $\sim 15\%$.

In addition, we compute model performance with respect to each land cover class based on the f1-score (per class) metric (see Fig. 3). Overall, the highest f1-score per land cover class is achieved when the three datasets are fused in the CNN & DF framework, whereas the lowest score is observed with DEM datasets in isolation. Moreover, other DF alternatives lead to high accuracies especially between wetland classes. The highest f1-scores among the land cover classes are observed in woody (90.43%) and emergent herbaceous wetlands (99.37%) with ARD + NAIP + DEM. These scores are closely followed by ARD + DEM with a difference of $\sim 1\%$. Note that ARD achieves moderate to high accuracies for woody (74.28%) and emergent herbaceous wetlands (93.42%) as compared to NAIP and DEM in isolation. The latter suggests that the LCC model can still achieve reasonable accuracies between wetlands classes in the absence of NAIP and generic DEM datasets (see Table II).

Regarding the other land cover classes, the model achieves moderate to very high f1-scores for open water (89.69% and 99.75%) and moderate to high scores for pasture/crops

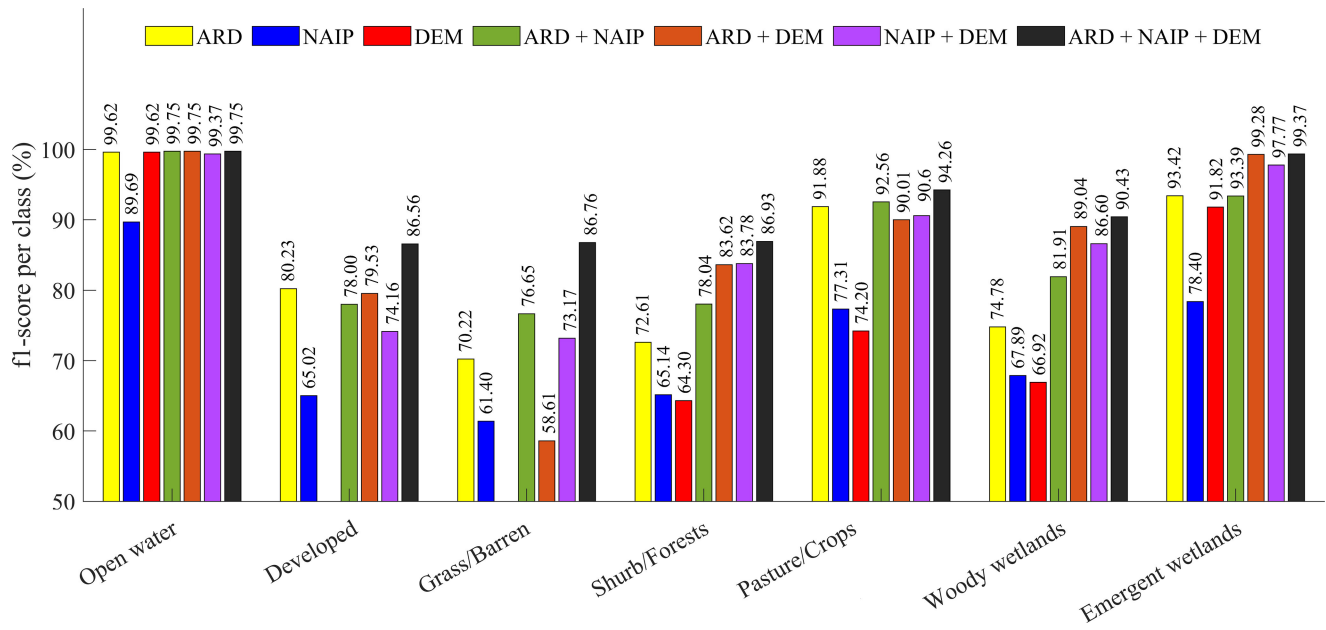


Fig. 3. Comparison of land cover classification accuracies (f1-score per class) between datasets with/out data fusion (DF) alternatives (years 2006, 2011 and 2013). Fusing Landsat ARD, NAIP, and generic DEM data (black bars) lead to the highest f1-score for all land cover classes and among the DF alternatives. ARD dataset (yellow bar) achieves the highest f1-scores with respect to the other datasets in isolation (red and blue bars). Note that DEM dataset (red bar) cannot identify developed and grass/barren land classes which in turn highlights the importance of accounting for spatial-spectral properties derived from either satellite or airborne imagery.

(74.20% and 94.26%) with/out DF alternatives, respectively. Shrub/forests exhibit a lower f1-score (65.14%) than the previous land cover classes, but this score improves by more than 13% when using DF alternatives. Similarly, the model achieves moderate f1-scores for developed (86.56%) and grass/barren land (86.76%) when the three datasets are fused in the CNN & DF framework. However, note that DEM dataset in isolation cannot identify those two land cover classes which is likely attributed to a broad range of elevation features (i.e., heights) especially in developed areas as reported in urban land cover classification studies [30], [31]. Specifically, we noticed that more than 80% of developed and grass/barren samples are incorrectly classified as shrub/forest and woody wetlands. Nevertheless, ARD and NAIP either in isolation or fused with DEM data help improve f1-scores in more than 60%.

Next to OAs and f1-scores, we compute confusion matrices of the datasets with/out DF alternatives and analyze misclassification errors of the CNN & DF framework. Particularly, we show the confusion matrix of ARD+NAIP+DEM with both producer's and user's accuracies at the bottom and right panels (see Table VII in the Appendix). Overall, both producer's and user's accuracies are above 80% suggesting that the number of patch images (samples) omitted and erroneously included in a given land cover class are relatively small compared to the multiannual sample size (e.g., 2006, 2001, and 2013). Analyses per wetland class reveal that both accuracies are even higher than most of the other land cover classes with almost a perfect score for emergent herbaceous wetlands (e.g., producer's acc.: 99.64% and user's acc. 99.10%). Woody wetlands are classified with moderate (87.72%) and high accuracies (93.32%), but misclassification errors are particularly observed in shrub/forest classes

due to similar spectral and elevation features. Specifically, 85 shrub/forest patch images are omitted from woody wetland class (omission error), whereas 40 shrub/forest patch images are erroneously classified as woody wetlands (commission error).

B. Model Performance and Accuracy Assessment

We generate 29 land cover maps of the Mobile Bay watershed [see Fig. 4(a)] and conduct geo-spatial analyses with annual, five-year interval and long-term data (1984–2019). As an illustration, wetland cover change between 1984 and 2019 [see Fig. 4(b)] is presented with three nomenclature levels to map gain, loss, and “no change” areas. Note that woody wetland coverage has expanded more in Baldwin than Mobile County and remained without change in the surrounding areas of Bon Secour Bay and Weeks Bay. Likewise, emergent wetland loss is evident along the shoreline of Baldwin County, whereas no major change of wetland coverage is observed near to Fort Morgan. Estimates of wetland area including percentage changes in Mobile Bay watershed (see Table IV) reveal an increase of woody wetlands (37.73%) and a reduction of emergent herbaceous wetlands (29.22%) between 1984 and 2019. Woody and emergent herbaceous wetlands have a net gain of 66.58 km² and loss of 13.01 km², respectively. Nevertheless, annual wetland areas exhibit sharp fluctuations regardless of the wetland class as these estimates depend on dataset time acquisition along with physical factors driven those fluctuations. Estimates of wetland cover change in a five-year interval (see Fig. 5) point out three major wetland losses in the period 1994–1998 (47.68 km²), 2005–2009 (56.01 km²), and 2010–2014 (45.75 km²) and two major gains in the period 1989–1993 (89.89 km²) and 2015–2019

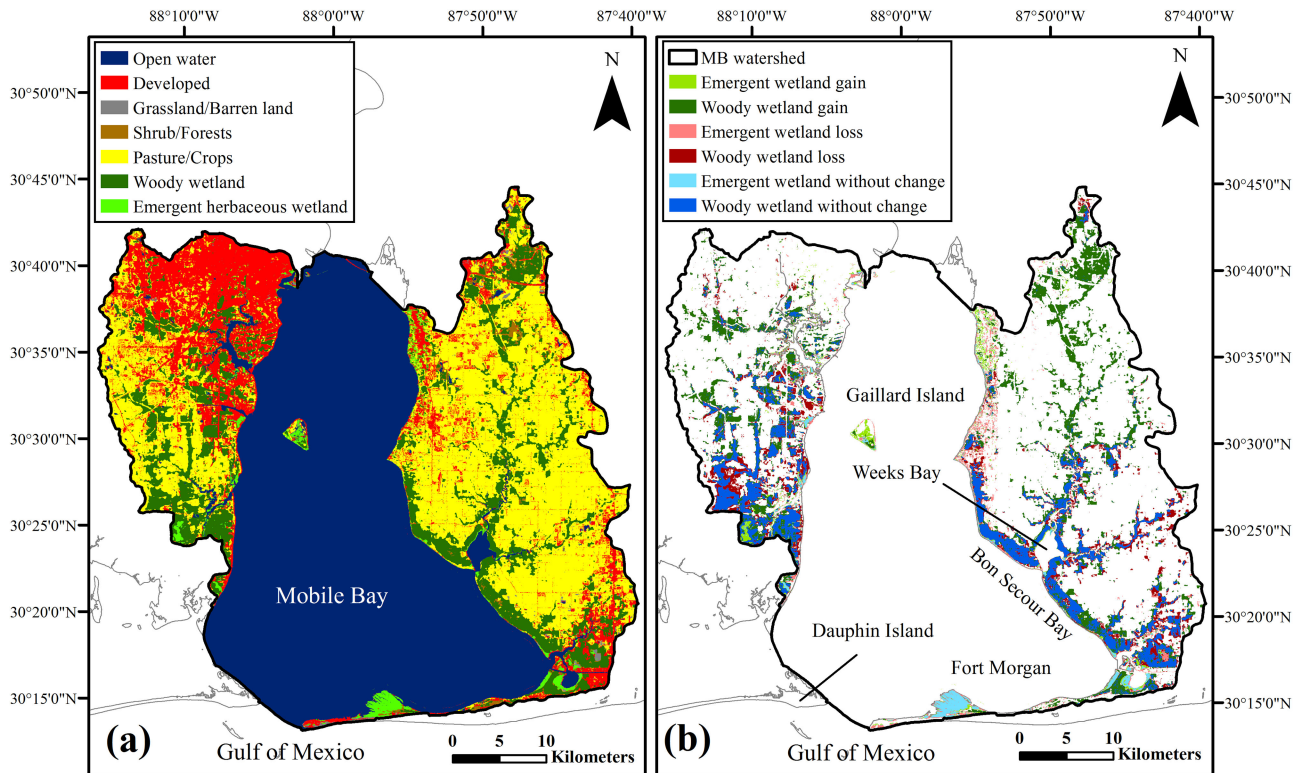


Fig. 4. Land cover map and wetland cover change analysis in Mobile Bay watershed, AL. (a) Land cover map of 2019 derived from the CNN & DF framework, and (b) long-term wetland cover change with respect to 1984 classified into wetland gain (green color scale), loss (red color scale), and no change (blue color scale). Total wetland gain for the period 1984–2019 exceeds wetland losses and accounts for 53.57 km².

TABLE IV
WETLAND COVER ESTIMATES IN MOBILE BAY WATERSHED FOR SELECTED YEARS IN km². PERCENTAGE CHANGES RELATIVE TO 1984 ARE SHOWN IN PARENTHESES

Wetland class	1984	1989	1994	1999	2004	2009	2014	2019
	[km ²]							
Woody	176.48	125.47 (-28.90)	219.89 (24.60)	230.55 (30.64)	224.60 (27.27)	46.47 (-73.67)	185.13 (4.90)	243.06 (37.73)
Emergent herbaceous	44.52	83.33 (87.18)	64.14 (44.08)	44.07 (-1.01)	45.96 (3.25)	62.19 (39.70)	45.90 (3.10)	31.51 (-29.22)
Total wetlands	220.99	208.80 (-5.52)	284.03 (28.52)	274.62 (24.26)	270.56 (22.43)	108.66 (-50.83)	231.03 (4.54)	274.57 (24.24)

(115.91 km²). The latter is mainly attributed to urban development, SLR, and hurricane impacts on wetland coverage as discussed in the next section.

C. Effects of Urbanization, SLR, and Hurricane Impacts on Wetland Cover Change

Results of total wetland balance in Mobile Bay watershed are shown for five-year intervals and long-term (see Fig. 5 and Table V). Likewise, Fig. 6(a) shows hurricane landfall dates and linear trends of developed class (urbanization) and open water class (SLR) to better visualize the effects of these drivers on wetland dynamics. In the first interval (1984–1988), Hurricane Elena (Sep/1985) affected Mobile Bay causing structural damage in houses with strong winds (~201 km/h) and a peak storm-surge (~1 m relative to NAVD88) recorded in Dauphin Island (NOAA station ID: 8735180). Urbanization and SLR

did not lead to wetland loss in contrast to the remaining land cover classes (see Table V). We estimate a net gain of 4.08 km² in emergent herbaceous wetlands despite the strong winds of Hurricane Elena. In the second interval, the state of Alabama did not report major hurricanes and urban development did not alter natural wetland expansion. However, note that open water areas (as a proxy of rising sea levels) reduced wetland gain compared to the previous interval. In fact, Fig. 6(a) shows that the mean sea level (MSL) within the second interval (1989–1993) is ~4 cm higher than the previous years [58]. Nonetheless, we estimate a net gain of 89.89 km² attributed to woody wetland expansion (see Fig. 5).

The third interval comprises Hurricane Opal (Oct/1995), Danny (Jul/1997), and Georges (Sep/1998) which generated a peak storm-surge at Dauphin Island (~1.10 m), torrential rainfalls in Mobile and Baldwin counties (~930 mm), and a peak storm-surge at Fort Morgan (~3.60 m), respectively [59].

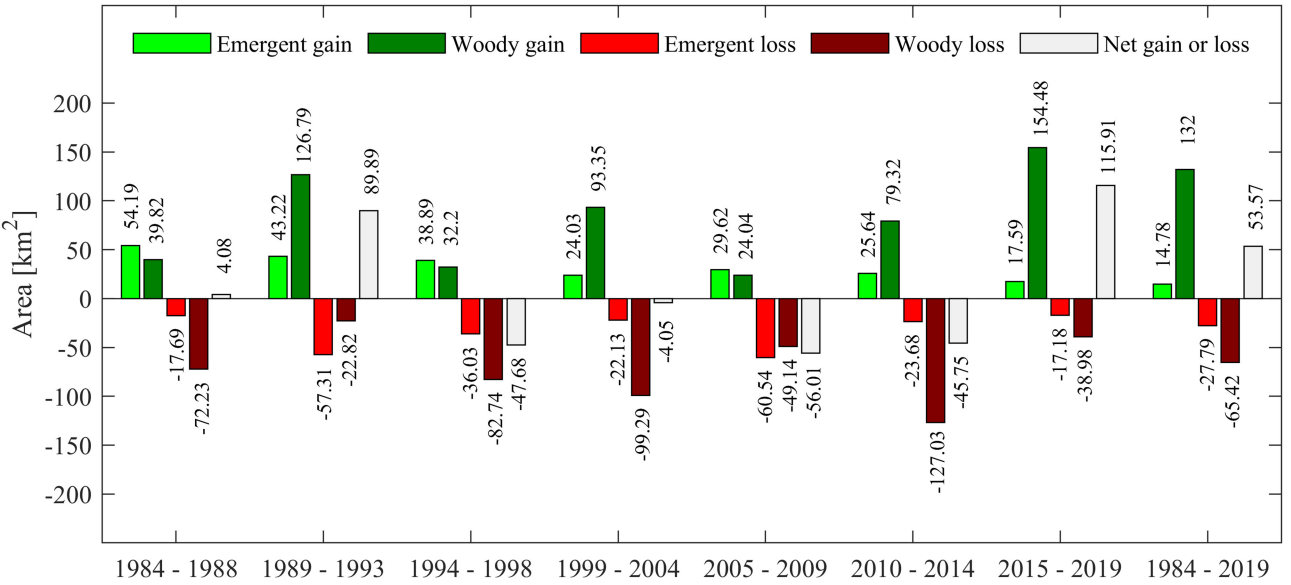


Fig. 5. Wetland cover change [km^2] in Mobile Bay watershed, AL for five-year intervals and long term (1984–2019). Wetland gain (green color scale) and loss (red color scale) estimates are computed for woody and emergent herbaceous wetlands separately. Total wetland (net) gain or loss is shown with light-gray bars.

TABLE V
WETLAND LOSS/GAIN ESTIMATES ATTRIBUTED TO URBAN DEVELOPMENT (U),
SEA LEVEL RISE (S) AND HURRICANE IMPACTS (IMPLICIT IN S AND C) IN
FIVE-YEAR INTERVALS AND LONG-TERM (1984–2019). NET RESIDUALS ARE
SHOWN IN PARENTHESES

Intervals	Urbanization (U)	SLR (S)	Other land cover classes (C)	Total wetland balance (Tw)
1984 – 1988	-15.34/18.08 (2.74)	-1.11/3.07 (1.95)	-73.47/72.86 (-0.61)	-89.92/94.01 (4.08)
1989 – 1993	-12.87/21.29 (8.42)	-3.67/4.07 (0.40)	-63.59/144.66 (81.07)	-80.13/170.02 (89.89)
1994 – 1988	-25.28/12.32 (-12.95)	-3.89/3.10 (-0.79)	-89.60/55.67 (-33.94)	-118.77/71.09 (-47.68)
1999 – 2004	-14.62/30.54 (15.92)	-3.99/3.32 (-0.67)	-102.82/83.52 (-19.30)	-121.43/117.38 (-4.05)
2005 – 2009	-33.19/10.13 (-23.06)	-1.01/2.60 (1.59)	-75.48/40.93 (-34.54)	-109.68/53.66 (-56.01)
2010 – 2014	-33.57/7.82 (-25.75)	-5.92/1.34 (-4.58)	-111.22/95.8 (-15.42)	-150.71/104.96 (-45.75)
2015 – 2019	-10.69/12.58 (1.89)	-0.89/2.69 (1.80)	-44.58/156.80 (112.22)	-56.16/172.07 (115.91)
1984 – 2019	-26.67/19.71 (-6.96)	-4.47/3.53 (-0.95)	-62.07/123.54 (61.48)	-93.21/146.78 (53.57)

Wetland loss as a result of urbanization, SLR, and “other land cover classes” [i.e., variable C in (1)] is apparent in this interval. We estimate that the compound effect of these drivers on wetland coverage led to a net loss of 47.68 km^2 ; particularly in woody wetlands that mostly became other land cover classes (see Table V). The next interval (1999–2004) comprises Hurricane Ivan (Sep/2004) that made landfall in Alabama and caused a peak storm-surge at Dauphin Island ($\sim 1.98 \text{ m}$). Wetland loss in this interval is attributed to SLR and other land cover classes despite a wetland gain in developed areas (e.g., upland wetland migration over “open space” areas). We estimate a net loss of 4.05 km^2 attributed to woody wetland expansion.

The fifth interval comprises Hurricane Katrina (Aug/2005) which considered one of the most damaging and costliest hurricanes that hit the Gulf of Mexico. Although Katrina made

landfall at $\sim 100 \text{ km}$ from Mobile Bay, the bay was exposed to a peak storm-surge ($\sim 1.79 \text{ m}$) and strong winds ($\sim 100 \text{ km/h}$) measured in Dauphin Island. In this interval, wetland loss as a result of urbanization and other land cover classes exceeds wetland gain in open water areas. We estimate a net loss of 56.01 km^2 in both woody and emergent herbaceous wetlands. Note that this is the largest net loss in the Mobile Bay watershed since 1984 (see Fig. 5). Urbanization, SLR, and other land cover classes caused wetland losses simultaneously in the next interval (2010–2014). Although this interval lacks hurricane threats, we estimate a net loss of 45.75 km^2 in woody wetlands with urbanization being the primary driver of wetland loss (see Table V). This net loss is comparable to the wetland losses estimated for Hurricane Opal, Danny, and Georges (second interval) and Hurricane Katrina (fifth interval). The last interval (2015–2019) comprises Hurricane Nate (Oct/2017) which caused a peak storm-surges measured at Dauphin Island ($\sim 1.21 \text{ m}$) and urban flooding in downtown Mobile. Urbanization and SLR did not alter wetland expansion over developed and open water areas, respectively. We estimate a net gain of 115.91 km^2 in both woody and emergent wetlands; primarily attributed to wetland migration toward upland areas (see Table V).

V. DISCUSSION

The effects of urbanization, SLR, and hurricane impacts on wetland dynamics led to a net gain of 53.57 km^2 (3.11%) of total wetlands between 1984 and 2019 (see Fig. 5 and Table V). This net gain is attributed to woody wetland expansion of 66.58 km^2 (37.73%) that exceeds emergent herbaceous wetland loss of 13.01 km^2 (29.22%) relative to 1984 (see Table IV). However, Fig. 6(b) shows that the long-term trend of emergent herbaceous wetlands ($\sim -2488 \text{ m}^2/\text{yr}$) is almost twice the magnitude of that of woody wetlands ($\sim 1383 \text{ m}^2/\text{yr}$). This in turn explains the

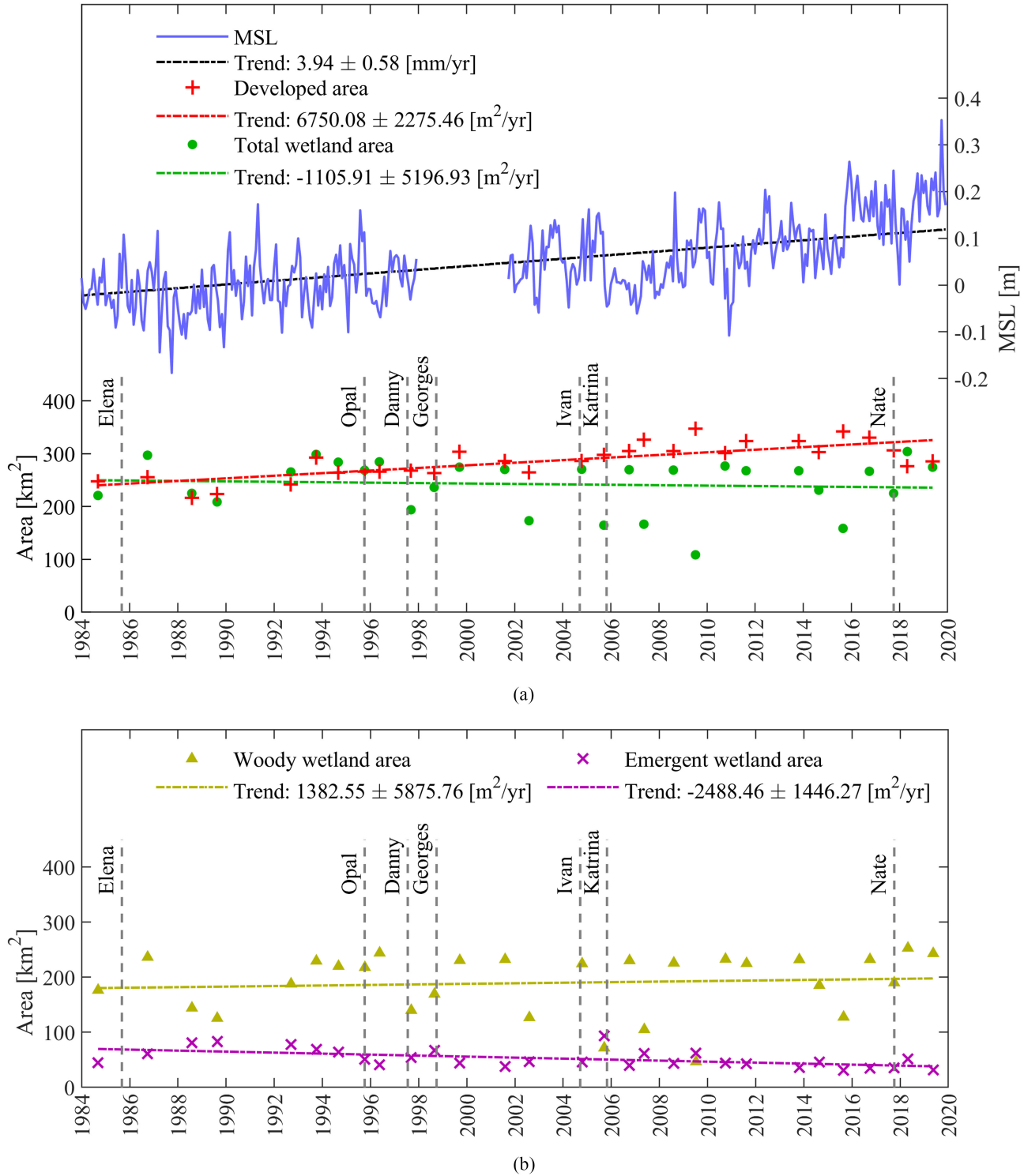


Fig. 6. Drivers of wetland dynamics in the Mobile Bay watershed, AL including long-term linear trends with 95% confidence intervals. (a) Monthly mean sea level (MSL) without seasonal fluctuations measured at Dauphin Island (blue solid line) and positive trend reflect a rise of sea level (~ 0.14 m) between 1984 and 2019. Developed area (red crosses) shows a positive trend suggesting urban expansion in the Mobile Bay watershed, whereas the total wetland area (green dots) shows a negative trend indicating wetland loss in the past 35 years. (b) Woody (yellow triangles) and emergent herbaceous (purple crosses) wetlands show a positive and negative trend, respectively. Note that the long-term trend of emergent wetlands is almost twice as large as that of woody wetlands, and thereby resulting in a negative trend of total wetland area. The main hurricanes that hit Alabama (gray dashed line) are included to visualize their effects on wetland cover change.

negative trend of total wetland area observed in the 35-year period [see Fig. 6(a)]. These results are in line with the findings of Ellis *et al.* [21] as they found a net gain of 16.6 km² (0.20%) attributed to woody wetlands. Note that they conducted geo-spatial analyses in a broader study area comprising Mobile and Baldwin counties and with Landsat imagery in the period 1974–2008. The decline in emergent herbaceous wetlands in the Mobile Bay watershed is also consistent with losses observed in nearby regions [60], [61], and is occurring at a similar rate than that of the world's wetlands [62].

These losses have important implications for the highly valuable ecosystem services that wetlands provide, namely carbon sequestration and nutrient removal [63]. In particular, emergent herbaceous wetlands sustain some of the highest rates of carbon sequestration due to their high productivity and ability to store organic carbon in the anoxic sediments. Losses of these ecosystems will therefore reduce their ability to sequester carbon and result in the release of millennial carbon stocks stored in the sediments to the open waters where it can be mineralized. Ellis *et al.* [21] indicated that urbanization reduced the total wetland extent in the vicinity of Mobile Bay by 13.90 km². Similarly, we estimate that urban development led to a net loss of 6.96 km² relative to 1984 (see Table V). Urban development has been expanding in the Mobile Bay watershed [see Fig. 6(a)] especially in Baldwin county where population growth, as an indirect measure of urbanization rate, has increased by 22.5% from 2010 to 2019 [64]. The increasing pace of urbanization in the Mobile Bay watershed will limit the ability of wetlands to migrate toward upland due to SLR, and will reduce their capacity to provide the highly valued ecosystems services.

SLR is likely to accelerate by the end of the 21st century at local and global scales under future climate scenarios [65], [66]. Mean sea level in Mobile Bay has been rising at a rate of 3.94 ± 0.58 mm/yr (95% confidence interval) according to monthly MSL records (1966–2020) at Dauphin Island gauge station [58]. Fig. 6(a) shows an increase of ~ 0.14 m in MSL between 1984 and 2019 which might explain a wetland net loss of 0.95 km² into open water (see Table V). The open water class is used as a proxy of SLR and involves complex processes such as salinization, sediment deposition, and nutrient availability. Table V shows that SLR fluctuates over time leading to a wetland loss in most of the intervals. Nevertheless, wetland gain over existing open water areas points out to the ability of emergent herbaceous wetlands to cope with SLR by controlling the overall sediment balance of marsh platforms. The conversion of these wetlands to subtidal unvegetated sediments will also significantly reduce their nutrient removal capacity [67]. Nutrients that would have otherwise been trapped and removed are instead exported to the nearshore waters where they contribute to eutrophication resulting in hypoxia [68] and blooms of harmful algae [69].

We argue that hydrodynamic modeling in addition to DL techniques are required to fully understand wetland dynamics especially in terms of marsh equilibrium with SLR. Alizad *et al.* [17] investigated coastal wetland response (i.e., salt marsh and/or emergent herbaceous) to SLR with Hydro-MEM model in Weeks Bay, AL. The authors reported a seven-fold increase

of salt marsh coverage by the end of the 21st century based on an intermediate-low SLR scenario (0.50 m). Such an increase was attributed to fluvial sediment inputs and suitable topography in Weeks Bay that help the marsh platform to accrete and keep pace with rising sea levels. Although our results show a decreasing trend of total wetland area [see Fig. 6(a)] and a more frequent emergent wetland loss than gain in annual basis and five-year intervals (see Table IV and Fig. 5), we infer that discrepancies with the results of Alizad *et al.*, [17] are associated with study area extent differences (e.g., Mobile Bay watershed versus Weeks Bay) and the fact that both urban development and hurricane impacts were not included in their analysis. In addition, note that the long-term trends of total wetland and developed area are based on 29 effective land cover maps leading to wide 95% confidence intervals. Nonetheless, our results are in line with those of Ellis *et al.*, [21] as they reported emergent wetland loss in Mobile Bay relative to 1974.

VI. CONCLUSION

We investigated wetland dynamics in Mobile Bay watershed, AL associated with urban development, SLR, and hurricane impacts between 1984 and 2019. For this purpose, we developed a LCC model that leverages state-of-the-art CNNs and DF techniques. The CNN & DF framework is aimed at processing readily available satellite-based (Landsat ARD) and airborne (NAIP) imagery including generic LiDAR-derived DEMs corrected for wetland elevation correction. The model achieved the highest accuracies when ARD, NAIP, and DEMs are fused in the CNN & DF framework, and also proved suitability for long-term wetland cover change analysis as compared to traditional ML and DL models that rely on single input data sources. Furthermore, the CNN & DF framework can be adapted to incorporate additional datasets such as radar and hyperspectral imagery, and thus reduce misclassification errors among other land cover classes.

Between 1984 and 2019, wetland cover change analyses reveal an increase of woody wetlands and a reduction of emergent herbaceous wetlands resulting in an overall net gain of 53.57 km² (3.11%). However, the long-term trend of emergent herbaceous wetlands (~ -2488 m²/yr) is almost twice as large as that of woody wetlands (~ 1383 m²/yr), and thereby resulting in a negative trend of total wetland coverage (~ 1106 m²/yr). Estimates of annual wetland coverage during leaf-on conditions (i.e., growing season) show sharp fluctuations partly explained by imagery acquisition time and the effects of hurricane impact on wetland coverage. The interval encompassing Hurricane Katrina (2005–2009) led to the largest wetland loss of 56.01 km² in the Mobile Bay watershed since 1984. Conversely, the most recent interval (2014–2019) led to the largest wetland gain of 115.91 km²; primarily attributed to wetland migration toward upland areas. The effects of SLR on wetland coverage are investigated in terms of open water class change (i.e., gain or loss from/to wetland classes), which led to a wetland loss in most of the 5-year intervals and the long-term period (35-year). Integration of DL, hydrodynamic, and statistical models is recommended for future research in order to fully understand wetland dynamics, especially the compound effects of SLR and hurricane impacts.

APPENDIX

TABLE VI
LAYERS OF THE CONVOLUTIONAL NEURAL NETWORK AND DATA FUSION FRAMEWORK

Description	Layer type	Input shape	Output shape
Imagery datasets	Input	(30, 30, 3)	-
Initial normalization	Batch normalization	(30, 30, 3)	(30, 30, 3)
	Conv2D + ReLU	(30, 30, 3)	(30, 30, 64)
	Batch normalization	(30, 30, 64)	(30, 30, 64)
Layer set 1	Avg2D pooling	(30, 30, 64)	(30, 30, 64)
	...	(30, 30, 64)	(30, 30, 64)
	...	(30, 30, 64)	(30, 30, 64)
Layer set 2	Point-wise addition	(30, 30, 64) x 3	(30, 30, 64)
	...	(30, 30, 64)	(30, 30, 64)
	...	(30, 30, 64)	(30, 30, 64)
Layer set 3	Adaptive feature-fusion approach
	FC	(1, 1, 64)	(1, 1, 64)
	FC + Sigmoid	(1, 1, 64)	(1, 1, 64)
Point-wise addition	Scalar multiplication	(30, 30, 64) : (1, 1, 64)	(30, 30, 64)
	...	(30, 30, 64) x 3	(30, 30, 192)
	...	(30, 30, 192)	(1, 1, 172800)
Data fusion	Concatenation	(30, 30, 64) x 3	(30, 30, 192)
Flatten	Flatten	(30, 30, 192)	(1, 1, 172800)
Dense layer	FC + ReLU	(1, 1, 172800)	(1, 1, 1024)
Drop neurons	Dropout	(1, 1, 1024)	(1, 1, 1024)
Classification	Softmax	(1, 1, 1024)	(1, 1, 7)

TABLE VII
CONFUSION MATRIX OF THE LAND COVER MODEL WITH FUSED LANDSAT ARD, NAIP, AND GENERIC DEM DATA (2006, 2011, AND 2013)
IN THE CNN & DF FRAMEWORK

Land cover class	Open water	Developed	Grass/barren	Shrub/forests	Crops/pasture	Woody wetland	Emergent wetland	User's acc. (%)
Open water	797	0	0	0	0	0	1	99.87
Developed	0	219	16	3	17	4	0	84.56
Grass/barren	1	5	213	9	21	0	0	85.54
Shrub/forests	0	4	4	552	10	85	0	84.27
Crops/pasture	0	15	7	11	681	1	0	95.24
Woody wetland	0	4	1	40	1	657	1	93.32
Emergent wetland	2	0	1	0	0	2	550	99.10
Producer's acc. (%)	99.63	88.66	88.02	89.76	93.29	87.72	99.64	OA: 93.24

ACKNOWLEDGMENT

The authors would like to thank the reviewers for their thoughtful comments that helped improve the quality of this work.

REFERENCES

- [1] L. M. Cowardin, *Classification of Wetlands and Deepwater Habitats of the United States*. Fish and Wildlife Service, US Dept. Interior, Washington, DC, USA, 1979.
- [2] W. J. Mitsch and J. G. Gosselink, “The value of wetlands: Importance of scale and landscape setting,” *Ecological Econ.*, vol. 35, no. 1, pp. 25–33, Oct. 2000.
- [3] M. Land, K. Tonderski, and J. T. A. Verhoeven, “Wetlands as biogeochemical hotspots affecting water quality in catchments,” in *Wetlands: Ecosystem Services, Restoration and Wise Use*, S. An and J. T. A. Verhoeven, Eds. Cham, Switzerland: Springer, 2019, pp. 13–37.
- [4] J. T. A. Verhoeven, B. Arheimer, C. Yin, and M. M. Hefting, “Regional and global concerns over wetlands and water quality,” *Trends Ecol. Evol.*, vol. 21, no. 2, pp. 96–103, Feb. 2006.
- [5] B. Kayranli, M. Scholz, A. Mustafa, and Å. Hedmark, “Carbon storage and fluxes within freshwater wetlands: A critical review,” *Wetlands*, vol. 30, no. 1, pp. 111–124, Feb. 2010.
- [6] J. Pokorný, P. Hesslerová, H. Huryna, and D. Harper, “Indirect and direct thermodynamic effects of wetland ecosystems on climate,” in *Natural and Constructed Wetlands: Nutrients, Heavy Metals and Energy Cycling, and Flow*, J. Vymazal, Ed. Cham, Switzerland: Springer, 2016, pp. 91–108.
- [7] B. J. Wilson, B. Mortazavi, and R. P. Kiene, “Spatial and temporal variability in carbon dioxide and methane exchange at three coastal marshes along a salinity gradient in a northern gulf of mexico estuary,” *Biogeochemistry*, vol. 123, no. 3, pp. 329–347, Apr. 2015.
- [8] E. B. Barbier, “Chapter 27 - The Value of coastal wetland ecosystem services,” in *Coastal Wetlands*, G. M. E. Perillo, E. Wolanski, D. R. Cahoon, and C. S. Hopkinson, Eds. Amsterdam, The Netherlands: Elsevier, 2019, pp. 947–964.
- [9] O. P.-M. Costanza, M. Luisa Martinez, P. Sutton, S. J. Anderson, and K. Mulder, “The value of coastal wetlands for hurricane protection,” *AMBIO, J. Human Environ.*, vol. 37, no. 4, pp. 241–249, Jun. 2008.
- [10] D. F. Muñoz, H. Moftakhari, and H. Moradkhani, “Compound effects of flood drivers and wetland elevation correction on coastal flood hazard assessment,” *Water Resour. Res.*, vol. 56, no. 7, 2020, Art. no. e2020WR027544.
- [11] T. V. Wamsley, M. A. Cialone, J. M. Smith, J. H. Atkinson, and J. D. Rosati, “The potential of wetlands in reducing storm surge,” *Ocean Eng.*, vol. 37, no. 1, pp. 59–68, Jan. 2010.
- [12] S. An and J. Verhoeven, Eds., *Wetlands: Ecosystem Services, Restoration and Wise Use*. New York, NY, USA: Springer, 2019.
- [13] W. Wu, Y. Zhou, and B. Tian, “Coastal wetlands facing climate change and anthropogenic activities: A remote sensing analysis and modelling application,” *Ocean Coastal Manage.*, vol. 138, pp. 1–10, Mar. 2017.
- [14] T. E. Dahl, *Status and Trends of Wetlands in the Conterminous United States 2004 to 2009*. US Dept. Interior, US Fish Wildlife Service, Fisheries, Washington, DC, USA, 2011.
- [15] W. K. Michener, E. R. Blood, K. L. Bildstein, M. M. Brinson, and L. R. Gardner, “Climate change, hurricanes and tropical storms, and rising sea level in coastal wetlands,” *Ecological Appl.*, vol. 7, no. 3, pp. 770–801, 1997.
- [16] N. C. Davidson, “How much wetland has the world lost? Long-term and recent trends in global wetland area,” *Marine Freshwater Res.*, vol. 65, no. 10, pp. 934–941, 2014.
- [17] K. Alizad *et al.*, “Dynamic responses and implications to coastal wetlands and the surrounding regions under sea level rise,” *PLOS ONE*, vol. 13, no. 10, Oct. 2018, Art. no. e0205176.

- [18] M. L. Kirwan and J. P. Megonigal, "Tidal wetland stability in the face of human impacts and sea-level rise," *Nature*, vol. 504, no. 7478, Dec. 2013, Art. no. 7478.
- [19] R. A. Morton and J. A. Barras, "Hurricane impacts on coastal wetlands: A half-century record of storm-generated features from Southern Louisiana," *J. Coastal Res.*, vol. 27, no. 6A, pp. 27–43, Nov. 2011.
- [20] J. C. Rodgers, A. W. Murrah, and W. H. Cooke, "The impact of hurricane katrina on the coastal vegetation of the weeks bay reserve, Alabama from NDVI data," *Estuaries Coasts*, vol. 32, no. 3, pp. 496–507, May 2009.
- [21] J. T. Ellis, J. P. Spruce, R. A. Swann, J. C. Smoot, and K. W. Hilbert, "An assessment of coastal land-use and land-cover change from 1974–2008 in the vicinity of mobile bay, Alabama," *J. Coastal Conservation*, vol. 15, no. 1, pp. 139–149, Mar. 2011.
- [22] J. P. Spruce, J. C. Smoot, J. T. Ellis, K. Hilbert, and R. Swann, "Geospatial method for computing supplemental multi-decadal US coastal land use and land cover classification products, using Landsat data and C-CAP products," *Geocarto Int.*, vol. 29, no. 5, pp. 470–485, Jul. 2014.
- [23] D. Mao *et al.*, "National wetland mapping in China: A new product resulting from object-based and hierarchical classification of Landsat 8 OLI images," *ISPRS J. Photogrammetry Remote Sens.*, vol. 164, pp. 11–25, Jun. 2020.
- [24] J. R. C. Muñoz and H. Moftakhar, "Adjusting emergent herbaceous wetland elevation with object-based image analysis, random forest and the 2016 NLCD," *Remote Sens.*, vol. 11, no. 20, Jan. 2019, Art. no. 2346.
- [25] Z. Jiang, "Spatial structured prediction models: Applications, challenges, and techniques," *IEEE Access*, vol. 8, pp. 38714–38727, 2020.
- [26] M. Mahdianpari, B. Salehi, M. Rezaee, F. Mohammadimesh, and Y. Zhang, "Very deep convolutional neural networks for complex land cover mapping using multispectral remote sensing imagery," *Remote Sens.*, vol. 10, no. 7, Jul. 2018, Art. no. 7.
- [27] M. Carranza-García, J. García-Gutiérrez, and J. C. Riquelme, "A framework for evaluating land use and land cover classification using convolutional neural networks," *Remote Sens.*, vol. 11, no. 3, Jan. 2019, Art. no. 3.
- [28] Y. Li, H. Zhang, X. Xue, Y. Jiang, and Q. Shen, "Deep learning for remote sensing image classification: A survey," *WIREs Data Mining Knowl. Discov.*, vol. 8, no. 6, 2018, Art. no. e1264.
- [29] Y. Chen, C. Li, P. Ghamisi, X. Jia, and Y. Gu, "Deep fusion of remote sensing data for accurate classification," *IEEE Geosci. Remote Sens. Lett.*, vol. 14, no. 8, pp. 1253–1257, Aug. 2017.
- [30] Y. Xu *et al.*, "Advanced multi-sensor optical remote sensing for urban land use and land cover classification: Outcome of the 2018 IEEE GRSS data fusion contest," *IEEE J. Sel. Topics Appl. Earth Observ. Remote Sens.*, vol. 12, no. 6, pp. 1709–1724, Jun. 2019.
- [31] Q. Feng, D. Zhu, J. Yang, and B. Li, "Multisource hyperspectral and LiDAR data fusion for urban land-use mapping based on a modified two-branch convolutional neural network," *ISPRS Int. J. Geo-Inf.*, vol. 8, no. 1, Jan. 2019, Art. no. 1.
- [32] J. Hu, L. Shen, and G. Sun, "Squeeze-and-excitation networks," in *Proc. IEEE Conf. Comput. Vis. Pattern Recognit.*, 2018, pp. 7132–7141.
- [33] D. Pouliot, R. Latifovic, J. Pasher, and J. Duffe, "Assessment of convolution neural networks for wetland mapping with Landsat in the central canadian boreal forest region," *Remote Sens.*, vol. 11, no. 7, Jan. 2019, Art. no. 7.
- [34] L. Yang *et al.*, "A new generation of the United States National Land Cover Database: Requirements, research priorities, design, and implementation strategies," *ISPRS J. Photogrammetry Remote Sens.*, vol. 146, pp. 108–123, Dec. 2018.
- [35] J. E. Dobson, "NOAA coastal change analysis program (C-CAP): Guidance for regional implementation," NOAA, Washington, DC, USA, Tech. Rep. 123, 1995.
- [36] B. Dzwonkowski, K. Park, H. Kyung Ha, W. M. Graham, F. J. Hernandez, and S. P. Powers, "Hydrographic variability on a coastal shelf directly influenced by estuarine outflow," *Continental Shelf Res.*, vol. 31, no. 9, pp. 939–950, Jun. 2011.
- [37] W. W. Schroeder, "Riverine influence on estuaries: A case study," in *Estuarine Interactions*, M. L. Wiley, Ed. New York, NY, USA: Academic, 1978, pp. 347–364.
- [38] J. L. Dwyer, D. P. Roy, B. Sauer, C. B. Jenkinson, H. K. Zhang, and L. Lymburner, "Analysis ready data: Enabling analysis of the Landsat archive," *Remote Sens.*, vol. 10, no. 9, Sep. 2018, Art. no. 1363.
- [39] D. Phiri, J. Morgenroth, C. Xu, and T. Hermosilla, "Effects of pre-processing methods on Landsat OLI-8 land cover classification using OBIA and random forests classifier," *Int. J. Appl. Earth Observation Geoinf.*, vol. 73, pp. 170–178, Dec. 2018.
- [40] A. E. Maxwell, T. A. Warner, B. C. Vanderbilt, and C. A. Ramezan, "Land cover classification and feature extraction from National Agriculture Imagery Program (NAIP) orthoimagery: A review," *Photogrammetric Eng. Remote Sens.*, vol. 83, no. 11, pp. 737–747, Nov. 2017.
- [41] C. Hladik and M. Alber, "Accuracy assessment and correction of a LIDAR-derived salt marsh digital elevation model," *Remote Sens. Environ.*, vol. 121, pp. 224–235, Jun. 2012.
- [42] A. McClure, X. Liu, E. Hines, and M. C. Ferner, "Evaluation of error reduction techniques on a LIDAR-Derived salt marsh digital elevation model," *J. Coastal Res.*, pp. 424–433, Sep. 2015.
- [43] J. N. Rogers, C. E. Parrish, L. G. Ward, and D. M. Burdick, "Assessment of elevation uncertainty in salt marsh environments using discrete-return and full-waveform lidar," *J. Coastal Res.*, vol. 76, pp. 107–122, Dec. 2016.
- [44] S. Medeiros, S. Hagen, J. Weishampel, and J. Angelo, "Adjusting lidar-derived digital terrain models in coastal marshes based on estimated aboveground biomass density," *Remote Sens.*, vol. 7, no. 4, pp. 3507–3525, Apr. 2015.
- [45] V. V. Klemas, J. E. Dobson, R. L. Ferguson, and K. D. Haddad, "A coastal land cover classification system for the NOAA coastwatch change analysis project," *J. Coastal Res.*, vol. 9, no. 3, pp. 862–872, 1993.
- [46] M. Rezaee, M. Mahdianpari, Y. Zhang, and B. Salehi, "Deep convolutional neural network for complex wetland classification using optical remote sensing imagery," *IEEE J. Sel. Topics Appl. Earth Observ. Remote Sens.*, vol. 11, no. 9, pp. 3030–3039, Sep. 2018.
- [47] W. R. Tobler, "A computer movie simulating urban growth in the detroit region," *Econ. Geography*, vol. 46, pp. 234–240, Jun. 1970.
- [48] D. Guidici and M. L. Clark, "One-Dimensional convolutional neural network land-cover classification of multi-seasonal hyperspectral imagery in the San Francisco bay area, California," *Remote Sens.*, vol. 9, no. 6, Jun. 2017, Art. no. 6.
- [49] S. Ioffe and C. Szegedy, "Batch normalization: Accelerating deep network training by reducing internal covariate shift," Mar. 2015. Accessed: Aug. 20, 2020. [Online]. Available: <http://arxiv.org/abs/1502.03167>
- [50] X. Glorot and Y. Bengio, "Understanding the difficulty of training deep feedforward neural networks," in *Proc. 13th Int. Conf. Artif. Intell. Statist.*, 2010, pp. 249–256.
- [51] G. E. Hinton, N. Srivastava, A. Krizhevsky, I. Sutskever, and R. R. Salakhutdinov, "Improving neural networks by preventing co-adaptation of feature detectors," Jul. 2012, Accessed: Aug. 21, 2020. [Online]. Available: <https://arxiv.org/abs/1207.0580v1>
- [52] NLCD, "National land cover database 2016 (NLCD2016) legend | multi-resolution land characteristics (MRLC) consortium," 2016. Accessed: Sep. 24, 2020. [Online]. Available: <https://www.mrlc.gov/data/legends/national-land-cover-database-2016-nlcd2016-legend>
- [53] R. A. Feagin, M. L. Martinez, G. Mendoza-Gonzalez, and R. Costanza, "Salt marsh zonal migration and ecosystem service change in response to global sea level rise: A case study from an urban region," *Ecol. Soc.*, vol. 15, no. 4, 2010, Accessed: Feb. 14, 2019. [Online]. Available: <https://www.jstor.org/stable/26268206>
- [54] N. W. Schieder, D. C. Walters, and M. L. Kirwan, "Massive upland to wetland conversion compensated for historical marsh loss in chesapeake bay, USA," *Estuaries Coasts*, vol. 41, no. 4, pp. 940–951, Jun. 2018.
- [55] K. Alizad, S. C. Hagen, J. T. Morris, S. C. Medeiros, M. V. Bilskie, and J. F. Weishampel, "Coastal wetland response to sea-level rise in a fluvial estuarine system," *Earth's Future*, vol. 4, no. 11, pp. 483–497, 2016.
- [56] M. L. Kirwan, D. C. Walters, W. G. Reay, and J. A. Carr, "Sea level driven marsh expansion in a coupled model of marsh erosion and migration," *Geophysical Res. Lett.*, vol. 43, no. 9, pp. 4366–4373, 2016.
- [57] L. M. Schile, J. C. Callaway, J. T. Morris, D. Stralberg, V. T. Parker, and M. Kelly, "Modeling tidal marsh distribution with sea-level rise: Evaluating the role of vegetation, sediment, and upland habitat in marsh resiliency," *PLOS ONE*, vol. 9, no. 2, Feb. 2014, Art. no. e88760.
- [58] NOAA, "Sea level trends - NOAA Tides & currents," 2020. Accessed: Aug. 10, 2020. [Online]. Available: https://tidesandcurrents.noaa.gov/slrends/slrends_station.shtml?id=8735180
- [59] NOAA-NHC, "National hurricane center," 2020. Accessed: Jan. 16, 2020. [Online]. Available: <https://www.nhc.noaa.gov/>
- [60] J. P. R. O'Donnell and J. F. Schalles, "Examination of abiotic drivers and their influence on spartina alterniflora biomass over a twenty-eight year period using Landsat 5 TM satellite imagery of the central georgia coast," *Remote Sens.*, vol. 8, no. 6, Jun. 2016, Art. no. 6.
- [61] Y. Sapkota and J. R. White, "Marsh edge erosion and associated carbon dynamics in coastal Louisiana: A proxy for future wetland-dominated coastlines world-wide," *Estuarine, Coastal Shelf Sci.*, vol. 226, Oct. 2019, Art. no. 106289.

- [62] R. C. Gardner and C. Finlayson, "Global wetland outlook: State of the world's wetlands and their services to people," SSRN Scholarly Paper, Art. no. 3261606, Oct. 2018. Accessed: Sep. 29, 2020. [Online]. Available: <https://papers.ssrn.com/abstract=3261606>
- [63] R. Costanza *et al.*, "The value of the world's ecosystem services and natural capital," *Nature*, vol. 387, no. 6630, pp. 253–260, May 1997.
- [64] U.S. Census Bureau, "U.S. Census Bureau quickfacts: United States," 2020. Accessed: Aug. 10, 2020. [Online]. Available: <https://www.census.gov/quickfacts/fact/table/mobilecountyalabama,baldwincountyalabama/PST045219>
- [65] R. E. Kopp *et al.*, "Probabilistic 21st and 22nd century sea-level projections at a global network of tide-gauge sites," *Earth's Future*, vol. 2, no. 8, pp. 383–406, Jun. 2014.
- [66] M. D. Palmer *et al.*, "Exploring the drivers of global and local sea-level change over the 21st century and beyond," *Earth's Future*, vol. 8, no. 9, 2020, Art. no. e2019EF001413.
- [67] S. E. Hinshaw *et al.*, "Vegetation loss decreases salt marsh denitrification capacity: Implications for marsh erosion," *Environ. Sci. Technol.*, vol. 51, no. 15, pp. 8245–8253, Aug. 2017.
- [68] N. N. Rabalaiz and R. E. Turner, "Gulf of mexico hypoxia: Past, present, and future," *Limnol. Oceanography Bull.*, vol. 28, no. 4, pp. 117–124, 2019.
- [69] P. M. Glibert and J. M. Burkholder, "The complex relationships between increases in fertilization of the earth, coastal eutrophication and proliferation of harmful algal blooms," in *Ecology of Harmful Algae*, E. Granéli and J. T. Turner, Eds. Berlin, Germany: Springer, 2006, pp. 341–354.



David F. Muñoz received the civil engineer degree from the University of Cuenca, Cuenca, Ecuador, in 2013, the MSc. degree in hydrology and water resources from Wageningen University & Research, Wageningen, the Netherlands, in 2017. He is currently working toward the Ph.D. degree in civil, construction, and environmental engineering at the University of Alabama, Tuscaloosa, AL, USA.

He worked in civil engineering projects in Cuenca, Ecuador (2013–2015), and urban flood research at the University of Coimbra, Portugal (2017–2018). He is currently a Research Assistant with the Center for Complex Hydroystems Research (CCHR), University of Alabama. His research interests include hydrodynamic modeling of coastal and estuarine processes including compound flood hazards in natural and urban landscapes, machine and deep learning techniques, and data assimilation for accurate flood hazard characterization.

Mr. Muñoz is a member of the American Geophysical Union (AGU) and Alabama Water Institute (AWI). He was the recipient of the SENESCYT scholarship (2014) from the Ecuadorian government, ERASMUS+ grant (2017) from the European Commission, and the National Water Center Innovators Program Award (2019) from the Consortium of Universities for Advancement of Hydrologic Science (CUAHSI), and the National Oceanic and Atmospheric Administration (NOAA).



Paul Muñoz received the civil engineering degree from the University of Cuenca, Cuenca, Ecuador, in 2015, and the M.Sc. degree in water resources engineering from the Katholieke Universiteit Leuven, Leuven, Belgium and Vrije Universiteit Brussel, Brussels, Belgium, in 2018. He is currently working toward the Ph.D. degree in water resources in the University of Cuenca.

His research interests include the use of artificial intelligence for real-time hydrological applications such as flood and drought forecasting, the use of remote sensing products for retrieving reliable precipitation information, and the evaluation of high-resolution technologies for punctual estimation of precipitation.

Dr. Muñoz is a selected member of the young scientists programme from Integrated Research on Disaster Risk (IRDR), China. He has been awarded with several scholarships including the VLIR-UOS Award Scholarship to study in Belgium, and recently, a 2-year research grant from the German Academic Exchange Service to complement his doctoral studies at the Philipps-University Marburg in Germany.



Atieh Alipour was born in Iran in 1989. She received the B.S. degree in civil engineering from the University of Tabriz, Tabriz, Iran, in 2013. She is currently working toward the Ph.D. degree in civil and environmental engineering in the University of Alabama, Tuscaloosa, AL, USA, under the supervision of Prof. Hamid Moradkhani.

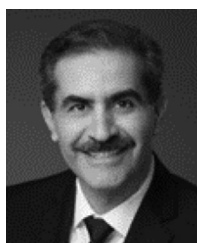
Since 2018, she has been a Research Assistant with the Center for Complex Hydroystems Research, University of Alabama. Her research interest includes hydrologic, hydrodynamic modeling, advanced statistical modeling, and artificial intelligence/machine learning.

Ms. Alipour is a member of the American Geophysical Union (AGU) and was selected as one of the eight 2019 NASA Data Visualization and Storytelling Competition Runner Up Winners. She also was the recipient of the Outstanding Student Presentation Award (OSPA) at the AGU 2018 Fall Meeting.



Hamed Moftakhar was born in Iran. He received the B.S. and M.S. degrees in 2007 and 2010, respectively, and received the Ph.D. degree in civil and environmental engineering from Portland State University, Portland, OR, USA, in 2015.

He was a Postdoctoral Scholar with the University of California, Irvine. His research is mainly on coastal hydrology and the impacts of compound and cascading hazards on people and assets located in low-lying coastal areas.



Hamid Moradkhani received the B.S. and M.S. degrees in water resources engineering and hydraulic structures, in 1991 and 1994, respectively, and the Ph.D. degree and postdoctoral fellowship in stochastic hydrology from the University of California, Irvine (UCI), Irvine, CA, USA, in 2004 and 2006, respectively.

He was a Professor of Civil and Environmental Engineering and the Director of Remote Sensing and Water Resources Lab at Portland State University (PSU), 2006–2017. He has been the Alton N. Scott Endowed Professor also

Endowed Professor also Hydraulics Professor at The University of Alabama, since 2018. He is Samuels School of Engineering's Hall of Fame at UCI, and honorary distinguished professor at Wuhan University. His research emphasis is on harnessing data revolution, predictive science, uncertainty analysis, machine learning, remote sensing, data assimilation, and high-performance computing. He is the Editor of AGU Earth's Future and on the Editorial Board of *Water Resources Research*, *Journal of Hydrology* and several other journals. He has authored more than 140 articles, book chapters, and proceedings and delivered over 50 keynotes and plenary speeches during his tenure.

Dr. Moradkhani a Fellow of the American Society of Civil Engineers, a Fellow of Environmental and Water Resources Institute, and a Diplomat of water resources engineering. He is the Editor of AGU Earth's Future and on the Editorial Board of *Water Resources Research*, *Journal of Hydrology* and several other journals. He was the recipient of several awards, including the American Association of Water Resources Engineers Outstanding Research and Innovation Award, Faculty Research Excellence Award, Branford P. Millar Award, for exceptional scholarship in research, instruction, university, and public service.



Behzad Mortazavi was born in Tehran, Iran, in 1969. He received the License and Maîtrise degrees in marine ecology from Université de P. & M. Curie, Paris, France, in 1992, and the Ph.D. degree in biological oceanography from The Florida State University, Tallahassee, FL, USA, in 1998.

From 1998 to 2007, he was an Assistant and Associate Research Scientist with Florida State University. Since 2008, he has been a Faculty with the Department of Biological Sciences, University of Alabama, Tuscaloosa, AL, USA, and is currently the Chair of the Department.

He was a Program Officer with the Directorate of Biological Sciences at the National Science Foundation during 2014–2015. He has published more than 48 articles. His work has been funded by the U.S. Department of Energy, the National Science Foundation, and The Gulf of Mexico Research Initiative (GoMRI). His research interests include biogeochemistry and use of stable isotopes to trace the transformation of nitrogen and carbon in the biosphere. Since the Deepwater Horizon oil spill in the Gulf of Mexico in 2010, he has been investigating the impact of the spill on saltmarsh biogeochemistry.